ELSEVIER

Journal of Computational and Applied Mathematics 91 (1998) 63–85

JOURNAL OF COMPUTATIONAL AND APPLIED MATHEMATICS

A spectral element method for the time-dependent two-dimensional Euler equations: applications to flow simulations [1]

Chuanju Xu [a,*], Yvon Maday [b]

[a] *Department of Mathematics, Xiamen University, Xiamen 361005, Fujian, China*

[b] *Laboratoire d'Analyse Numérique, Université Pierre et Marie Curie, Paris, France*

Received 1 April 1997

Abstract

A numerical spectral element method for the computation of fluid flows governed by the incompressible Euler equations in a complex geometry is presented. The appropriate elemental interface conditions for the velocity and the pressure are found by using variational formulation. It is proven that spectral approximations of same degrees for the velocity and the pressure, called $\mathbb{P}_N \times \mathbb{P}_N$ version, conduct to well-posed discrete problems, which is not true in general in the case of the Navier–Stokes equations. Applications to fluid flow simulation using the Navier–Stokes/Euler coupled model are presented.

AMS classification: 65M70 65M12 65N22 76C05

Keywords: Euler equations; Navier–Stokes equations; Domain decomposition; Spectral element methods

1. Introduction

It is well known [4, 5] that the spectral methods are competitive as compared with the methods more classical such as finite difference or finite element. This competitivity is clearly shown over the equations of elliptic or parabolic type where the solutions are in general regular. However the efficacity of the spectral methods has not been proven over the equations of hyperbolic type such as the incompressible Euler equations. The principal difficulty lies into the fact that the solutions of these equations are rarely regular.

* Coresponding author. E-mail: cjxu@xmu.edu.cn.

[1] This work was partially supported by State Commission of Education.

0377-0427/98/$19.00
PII S0377-0427(98)00022-3

In Ref. [13], we have studied a Galerkin-spectral method for approaching the two-dimensional Euler equations posed in a simple domain. If we want to treat a more complex and general domain, spectral element methods would have to be considered.

This paper deals with the evolutional incompressible Euler equations by a spectral element method. We will follow the splitting idea introduced in Ref. [13] for treating the nonlinear (convection) term. This splitting technique, which seems to have regularization effects over the solution, consists in decomposing the Euler equations

$$\frac{\partial \boldsymbol{u}}{\partial t} + \boldsymbol{u} \cdot \nabla \boldsymbol{u} + \nabla p = \boldsymbol{f}, \quad \nabla \cdot \boldsymbol{u} = 0. \tag{1}$$

into two classical problems: an elliptic problem in the velocity-pressure variable $(\boldsymbol{u}, P)$

$$\frac{\partial \boldsymbol{u}}{\partial t} + \omega \times \boldsymbol{u} + \nabla P = \boldsymbol{f}, \quad \nabla \cdot \boldsymbol{u} = 0 \tag{2}$$

and a transport problem in the vorticity variable ω

$$\frac{\partial \omega}{\partial t} + (\boldsymbol{u} \cdot \nabla)\omega = \nabla \times \boldsymbol{f} \tag{3}$$

where $\omega = \nabla \times \boldsymbol{u} = \partial u_2/\partial x_1 - \partial u_1/\partial x_2$ is the vorticity, $\omega \times \boldsymbol{u} = (-\omega u_2, \omega u_1)$, P is the total pressure. This split formulation allows us to separately find $(\boldsymbol{u}, P)$ and ω by using suitable time schema, for instance the following 1-order finite difference schema:

$$\frac{\boldsymbol{u}^{n+1} - \boldsymbol{u}^n}{\triangle t} + \omega^n \times \boldsymbol{u}^{n+1} + \nabla P^{n+1} = \boldsymbol{f}^{n+1}, \quad \nabla \cdot \boldsymbol{u}^{n+1} = 0 \tag{4}$$

completed by

$$\frac{\omega^{n+1} - \omega^n}{\triangle t} + (\boldsymbol{u}^{n+1} \cdot \nabla)\omega^{n+1} = \nabla \times \boldsymbol{f}^{n+1}. \tag{5}$$

As regards the issue of geometric generality, it is clear that with the introduction of macro-element and local mappings, spectral element methods can treat a wide class of geometrically and physically complex problems for which global spectral methods are not appropriate. We consider here a general geometry which is partitioned into a certain number of the subdomains (macro-elements). Each subdomain can be transformed to a square by a simple analytical mapping. The spectral element discretization in this kind of geometry consists essentially in treating the elemental interface conditions in a correct and easier way. Variational formulations permit us to generate the appropriate interface conditions in a natural way. We propose the discontinuous velocity/continuous pressure approximation for the $(\boldsymbol{u}, P)$ problem, Eq. (2), and the continuous vorticity approximation for the ω problem, Eq. (3). These approximations showed more evidence from the point of view of the Brezzi's "Inf-Sup" condition than the general approximations on the Navier–Stokes equations. It is well known that in the resolution of the Stokes-type equations the "Inf-Sup" condition is a difficult point to verify. By contrast in the spectral element approximation for the Euler equations proposed here, we can fulfill Brezzi's "Inf-Sup" condition in an easy way, both for the continuous problem and for the discrete one. Moreover we show that the constant of the "Inf-Sup" condition is

independent of the polynomial degree N. This is a very important characteristic which permits the simplification of all the numerical solvers.

We will introduce and analyze a spectral element method to approximate Eqs. (4) and (5). The method is validated by numerical tests which show good agreement with the theoretical analysis.

To show potential applications of our numerical method of solving Euler equations, we perform some simulations of fluid flow governed by the inviscid equations and also by the viscous equations. That is, we perform computation of fluid flow simulations based on our initial idea of coupling the incompressible Navier–Stokes and Euler equations in the context of spectral approximation [17]. The goal of these simulations is to prove the stability of the spectral element method proposed in this paper, and also to show its potential applications via a coupling strategy with the Navier–Stokes equations.

The outline of this paper is as follows. We start in Section 2 by reviewing the basic idea of Galerkin-spectral approximation for the Euler equations. In Section 3 we introduce and analyze the spectral element discretization. A particular attention focuses on the analysis of a post-treatment procedure. In Section 4 we discuss how these results extend to more complex geometry situations. Numerical examples are given in Section 5. Lastly, in Section 6 we present the results of some moderate Reynolds number unsteady flow simulation performed by using the Euler/Navier–Stokes coupled model.

1.1. Notation

Let Ω to be a bounded, connected, open subset of $\mathbb{R}^2$. For all $m \geqslant 0$, we denote by $H^m(\Omega)$ the classical Sobolev spaces, provided with the usual norm $\|\cdot\|_{m,\Omega}$, and also with the semi-norm $|\cdot|_{m,\Omega}$. We consider also the space $L^\infty(\Omega)$ with the norm $\|\cdot\|_{L^\infty(\Omega)}$. For any integer N, we denote $\mathbb{P}_N(\Omega)$ to be the set of all polynomials of degree $\leqslant N$ in Ω. In all that follows, we use letters of boldface type to denote vectors and vector functions. $C_0, C, C_1, \cdots$ are generic positive constants independent of discretization parameters N and $\triangle t$, but possibly dependent on the exact solutions of the equations under consideration.

2. Galerkin-spectral approximation

We first recall the main results concerning the Galerkin-spectral approximation of the Euler equations which were first presented in Ref. [13].

Let $\Omega = (-1,+1)^2$. For the sake of simplification, we consider the Euler equations with the homogeneous boundary condition $\boldsymbol{u}\cdot\boldsymbol{n} = 0$. The semi-discrete equations (4) can be rewritten as follows:

$$\begin{aligned} &\alpha\boldsymbol{u}^{n+1} + \omega^n \times \boldsymbol{u}^{n+1} + \nabla P^{n+1} = \alpha\boldsymbol{u}^n + \boldsymbol{f}^{n+1} && \text{in } \Omega, \\ &\nabla\cdot\boldsymbol{u}^{n+1} = 0 && \text{in } \Omega, \\ &\boldsymbol{u}^{n+1}\cdot\boldsymbol{n} = 0 && \text{on } \partial\Omega. \end{aligned} \tag{6}$$

where $\alpha = 1/\triangle t$.

The equivalent variational statement of Eq. (6) is: *Find* $(\boldsymbol{u}^{n+1}, P^{n+1}) \in L^2(\Omega)^2 \times (H^1(\Omega)/\mathbb{R})$ *such that*

$$\begin{aligned} &\alpha(\boldsymbol{u}^{n+1}, \boldsymbol{v}) + (\omega^n \times \boldsymbol{u}^{n+1}, \boldsymbol{v}) + (\nabla P^{n+1}, \boldsymbol{v}) = (\alpha \boldsymbol{u}^n + \boldsymbol{f}^{n+1}, \boldsymbol{v}) \quad \forall \boldsymbol{v} \in L^2(\Omega)^2, \\ &(\boldsymbol{u}^{n+1}, \nabla q) = 0 \qquad \forall q \in H^1(\Omega)/\mathbb{R}, \end{aligned} \tag{7}$$

where $(\cdot,\cdot)$ denotes the usual L^2-scalar product. Its Galerkin-spectral approximation is: *Find* $(\boldsymbol{u}_N^{n+1}, P_N^{n+1}) \in \mathbb{P}_N(\Omega)^2 \times (\mathbb{P}_N(\Omega)/\mathbb{R})$ *such that*

$$\begin{aligned} &\alpha(\boldsymbol{u}_N^{n+1}, \boldsymbol{v}) + (\omega_N^n \times \boldsymbol{u}_N^{n+1}, \boldsymbol{v}) + (\nabla P_N^{n+1}, \boldsymbol{v}) = (\alpha \boldsymbol{u}_N^n + \boldsymbol{f}^{n+1}, \boldsymbol{v}) \quad \forall \boldsymbol{v} \in \mathbb{P}_N(\Omega)^2, \\ &(\boldsymbol{u}_N^{n+1}, \nabla q) = 0 \qquad \forall q \in \mathbb{P}_N(\Omega)/\mathbb{R}, \end{aligned} \tag{8}$$

where ω_N^n is the discrete vorticity computed by a discrete transport equation.

Define the space V_N:

$$V_N = \{\boldsymbol{v} \in \mathbb{P}_N(\Omega)^2; (\boldsymbol{v}, \nabla q) = 0 \text{ for all } q \in \mathbb{P}_N(\Omega)/\mathbb{R}\}.$$

Let R_N to be the orthogonal projection operator from $L^2(\Omega)^2$ into V_N, and R_N' the orthogonal projection operator from $H^1(\Omega)$ into $\mathbb{P}_N(\Omega)$.

Theorem 2.1. *For all* $\omega_N^n \in L^\infty(\Omega)$, $\boldsymbol{u}_N^n \in L^2(\Omega)$, $\boldsymbol{f}^{n+1} \in L^2(\Omega)$, *the Problem* (8) *admits one unique solution. Furthermore, if* $(\boldsymbol{u}^{n+1}, P^{n+1})$ *and* $(\boldsymbol{u}_N^{n+1}, P_N^{n+1})$ *are respectively the solutions of Problems* (4) *and* (8), *then*

$$\begin{aligned} \alpha\|R_N\boldsymbol{u}^{n+1} - \boldsymbol{u}_N^{n+1}\|_{0,\Omega} \leqslant{}& \alpha\|R_N\boldsymbol{u}^n - \boldsymbol{u}_N^n\|_{0,\Omega} + \|R_N\boldsymbol{u}^{n+1}\|_{L^\infty(\Omega)}\|\omega^n - \omega_N^n\|_{0,\Omega} \\ &+ |P^{n+1} - R_N' P^{n+1}|_{1,\Omega} + \|\omega^n\|_{L^\infty(\Omega)}\|\boldsymbol{u}^{n+1} - R_N\boldsymbol{u}^{n+1}\|_{0,\Omega} \end{aligned}$$

and

$$\begin{aligned} \|\nabla(P^{n+1} - P_N^{n+1})\|_{0,\Omega} \leqslant{}& 2|P^{n+1} - R_N' P^{n+1}|_{1,\Omega} + (\alpha + \|\omega_N^n\|_{L^\infty(\Omega)})\|\boldsymbol{u}^{n+1} - \boldsymbol{u}_N^{n+1}\|_{0,\Omega} \\ &+ \|\boldsymbol{u}^n - \boldsymbol{u}_N^n\|_{0,\Omega} + \|\boldsymbol{u}^{n+1}\|_{L^\infty(\Omega)}\|\omega^n - \omega_N^n\|_{0,\Omega}. \end{aligned}$$

The Galerkin-spectral approximation of the semi-discrete equations (5) is: *Find* $\omega_N^{n+1} \in \mathbb{P}_N(\Omega)$, *such that for all* $z \in \mathbb{P}_N(\Omega)$,

$$\alpha(\omega_N^{n+1}, z) + ((\boldsymbol{u}_N^{n+1} \cdot \nabla)\omega_N^{n+1}, z) = (\alpha\omega_N^n + \nabla \times \boldsymbol{f}^{n+1}, z). \tag{9}$$

Remark 2.2. In the case of nonhomogeneous boundary condition $\boldsymbol{u} \cdot \boldsymbol{n} = \varphi \neq 0$, a well-posed spectral discrete problem would be

$$\alpha(\omega_N^{n+1}, z) + ((\boldsymbol{u}_N^{n+1} \cdot \nabla)\omega_N^{n+1}, z) - \int_{\Gamma_{\text{in}}} \varphi\omega_N^{n+1} z \, \mathrm{d}\sigma = (\alpha\omega_N^n + \nabla \times \boldsymbol{f}^{n+1}, z) - \int_{\Gamma_{\text{in}}} \varphi\psi z \, \mathrm{d}\sigma$$

where $\Gamma_{\text{in}} = \{\boldsymbol{x} \in \partial\Omega; \boldsymbol{u} \cdot \boldsymbol{n}(\boldsymbol{x}) < 0\}$, ψ is the "inflow" boundary condition, i.e., $\omega|_{\Gamma_{\text{in}}} = \psi$.

Theorem 2.3. *Let ω^{n+1} and ω_N^{n+1} respectively be the solutions of Problems* (5) *and* (9), *and let Q_N be the orthogonal projection from $L^2(\Omega)$ into $\mathbb{P}_N(\Omega)$. Then*

$$\begin{aligned}&[\alpha - CN^2\|\boldsymbol{u}^{n+1} - R_N\boldsymbol{u}^{n+1}\|_{L^\infty(\Omega)} - CN^4\|R_N\boldsymbol{u}^{n+1} - \boldsymbol{u}_N^{n+1}\|_{0,\Omega}]\|Q_N\omega^{n+1} - \omega_N^{n+1}\|_{0,\Omega}\\ &\quad\leqslant\alpha\|Q_N\omega^n - \omega_N^n\|_{0,\Omega} + \|\boldsymbol{u}^{n+1}\|_{L^\infty(\Omega)}\|Q_N\omega^{n+1} - \omega^{n+1}\|_{1,\Omega}\\ &\qquad+\|\nabla(Q_N\omega^{n+1})\|_{L^\infty(\Omega)}\|\boldsymbol{u}^{n+1} - \boldsymbol{u}_N^{n+1}\|_{0,\Omega}.\end{aligned}$$

Lemma 2.4. *For all $\boldsymbol{u}\in\{\boldsymbol{v}\in H^m(\Omega)^2;\ (\boldsymbol{v},\nabla q) = 0,\forall q\in H^1(\Omega)/\mathbb{R}$, all $p\in H^{m+1}(\Omega)$, and all $\omega\in H^m(\Omega)$, there exists a constant C independent of N, such that*

$$\begin{aligned}&\|\boldsymbol{u} - R_N\boldsymbol{u}\|_{0,\Omega}\leqslant CN^{-m}\|\boldsymbol{u}\|_{m,\Omega},\\ &|p - R_N'p|_{1,\Omega}\leqslant CN^{-m}\|p\|_{m+1,\Omega},\\ &\|\omega - Q_N\omega\|_{0,\Omega}\leqslant CN^{-m}\|\omega\|_{m,\Omega},\\ &\|\omega - Q_N\omega\|_{1,\Omega}\leqslant CN^{-m}\|\omega\|_{m+1,\Omega}.\end{aligned}$$

Lemma 2.5. *Let $\{a_n\}$, $\{b_n\}$ be two positive series, satisfying the recurrent relation*

$$a_{n+1}\leqslant a_n + C\,\triangle t\,b_n + \varepsilon_1^n, \tag{10}$$

$$(1 - C\,\triangle t - C\,\triangle t\,N^4a_{n+1})b_{n+1}\leqslant b_n + C\,\triangle t\,a_{n+1} + \varepsilon_2^n \tag{11}$$

ε_1^n, ε_2^n are two given series satisfying, for all positive integer $n < T/\triangle t$, $T > 0$:

$$\varepsilon_1^n\leqslant C\,\triangle t\,N^{-m},\qquad \varepsilon_2^n\leqslant C\,\triangle t\,N^{-m} \tag{12}$$

where m is a large enough integer ($m\geqslant 4$ at least). If $a_0\leqslant C_1N^{-m}, b_0\leqslant C_2N^{-m}$, then for all positive integer $n, n+1\leqslant T/\triangle t$, the following estimates hold:

$$a_{n+1} + b_{n+1}\leqslant C_3(a_0 + b_0 + N^{-m}). \tag{13}$$

From the above lemma and Theorems 2.1 and 2.3, we obtain the following results.

Corollary 2.6. *Assume $(\boldsymbol{u}^{n+1}, P^{n+1})$ and ω^{n+1} to be the solutions of Eqs.* (4) *and* (5), *$(\boldsymbol{u}_N^{n+1}, P_N^{n+1})$ and ω_N^{n+1} to be the solutions of Eqs.* (8) *and* (9). *Furthermore assume that there exists $m, m\geqslant 4$, such that $\boldsymbol{u}^{n+1}\in H^m(\Omega)^2$, $P^{n+1}\in H^{m+1}(\Omega)$, $\omega^{n+1}\in H^{m+1}(\Omega)$. Then for all positive integer $n, n+1\leqslant T/\triangle t$, $T > 0$,*

$$\begin{aligned}&\|\boldsymbol{u}^{n+1} - \boldsymbol{u}_N^{n+1}\|_{0,\Omega}\leqslant C(\|\boldsymbol{u}^0 - \boldsymbol{u}_N^0\|_{0,\Omega} + \|\omega^0 - \omega_N^0\|_{0,\Omega} + N^{-m}),\\ &\|\omega^{n+1} - \omega_N^{n+1}\|_{0,\Omega}\leqslant C(\|\boldsymbol{u}^0 - \boldsymbol{u}_N^0\|_{0,\Omega} + \|\omega^0 - \omega_N^0\|_{0,\Omega} + N^{-m}),\\ &|P^{n+1} - P_N^{n+1}|_{1,\Omega}\leqslant C\left(1 + \frac{1}{\triangle t}\right)(\|\boldsymbol{u}^0 - \boldsymbol{u}_N^0\|_{0,\Omega} + \|\omega^0 - \omega_N^0\|_{0,\Omega} + N^{-m}),\end{aligned}$$

where C depends on T and $\|\boldsymbol{u}\|_{m,\Omega}$, $\|P\|_{m+1,\Omega}$, $\|\omega\|_{m+1,\Omega}$.

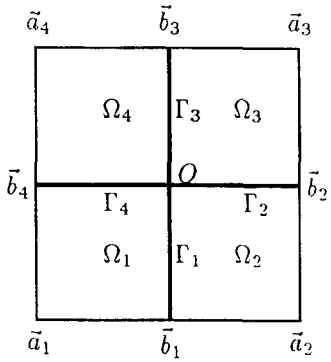

Fig. 1. An example of computational multidomain

Remark 2.7. In Corollary 2.6, we assume $\boldsymbol{u} \in H^m(\Omega)^2$, $m \geqslant 4$. This is a technical hypothesis which is needed only during the proof of Lemma 2.5. In fact the numerical experiments presented in Section 5 will show that this hypothesis is not really necessary for numerical solutions to be stable, and that accurate numerical solutions could also be obtained by increasing the polynomial degree even if the solutions to be approximated are of low regularity.

3. Spectral element discretization

In spectral element discretization we break Ω into K disjoint subdomains, and then approximate the dependent and independent variables by Nth-order polynomial expansions within the individual subdomains.

To fix the idea, first consider the case where Ω is the rectangular domain $(-2,+2)^2$ partitioned into 4 squares (see Fig. 1).

All the quantities defined in Ω_k $(k = 1,\ldots,K)$ are identified by an indice k. For example if φ is a function defined in Ω then the restriction of φ in Ω_k is denoted by φ_k. For k, $1 \leqslant k \leqslant K$, $\Xi_{N,k}$ denotes the set of the Gauss–Lobatto–Legendre points $(\xi^1_{i,k}, \xi^2_{j,k})$, $0 \leqslant i,j \leqslant N$ in Ω_k. $\Xi_N = \bigcup_{k=1}^K \Xi_{N,k}$. The corresponding weights in two spatial directions are denoted respectively by $w^1_{i,k}$ and $w^2_{j,k}$. Let $\xi^k_{ij} = (\xi^1_{i,k}, \xi^2_{j,k}), \omega^k_{ij} = w^1_{i,k} w^2_{j,k}$. For all φ, $\phi \in C^0(\Omega_k)$ define

$$(\varphi, \phi)_{N,k} = \sum_{i=0}^{N} \sum_{j=0}^{N} \varphi(\xi^k_{ij}) \phi(\xi^k_{ij}) w^k_{ij}, \quad k = 1,\ldots,K. \tag{14}$$

We recall that the quadratic formula:

$$\int_{\Omega_k} \varphi \, \mathrm{d}\boldsymbol{x} = \sum_{i=0}^{N} \sum_{j=0}^{N} \varphi(\xi^k_{ij}) w^k_{ij} \tag{15}$$

holds for all $\varphi \in \mathbb{P}_{2N-1}(\Omega_k)$, and that, for all $\varphi \in \mathbb{P}_N(\Omega_k)$ we have the inequality:

$$\int_{\Omega_k} \varphi^2 \, \mathrm{d}\boldsymbol{x} \leqslant \sum_{i=0}^{N} \sum_{j=0}^{N} \varphi^2(\xi^k_{ij}) w^k_{ij} \leqslant 9 \int_{\Omega_k} \varphi^2 \, \mathrm{d}\boldsymbol{x}. \tag{16}$$

According to inequality (16), the bilinear form (14) is uniformly equivalent to the L^2-scalar product in the space $\mathbb{P}_N(\Omega_k)$. Moreover, defining

$$Y_N = \{v; v_k \in \mathbb{P}_N(\Omega_k),\ \forall 1 \leqslant k \leqslant K\}$$

and the bilinear form

$$((\varphi, \phi))_N = \sum_{k=0}^{K} (\varphi, \phi)_{N,k}, \tag{17}$$

$((\varphi, \phi))_N$ is a scalar product in Y_N. If $\|\cdot\|_N$ the associated norm is noticed, then

$$\|\varphi\|_{0,\Omega} \leqslant \|\varphi\|_N \leqslant 3\|\varphi\|_{0,\Omega}, \quad \forall \varphi \in Y_N. \tag{18}$$

3.1. Elliptic problem on velocity-pressure $(\boldsymbol{u}, P)$

For purpose of simplification, hereafter we drop all time superscripts n.

Problem (7) can be written in the multidomain form: *Find* $(\boldsymbol{u}, P) \in L^2(\Omega)^2 \times (H^1(\Omega)/\mathbb{R})$ *such that, for all* $\boldsymbol{v} \in L^2(\Omega)^2$ *and* $q \in H^1(\Omega)/\mathbb{R}$,

$$\begin{aligned} &\sum_{k=1}^{K} \alpha(\boldsymbol{u}_k, \boldsymbol{v}_k)_k + (\omega \times \boldsymbol{u}_k, \boldsymbol{v}_k)_k + ((\nabla P)|_{\Omega_k}, \boldsymbol{v}_k)_k = \sum_{k=1}^{K} (\underline{\boldsymbol{f}}, \boldsymbol{v}_k)_k, \\ &\sum_{k=1}^{K} (\boldsymbol{u}_k, (\nabla q)|_{\Omega_k})_k = 0, \end{aligned} \tag{19}$$

where $\underline{\boldsymbol{f}} = \alpha \boldsymbol{u}^n + \boldsymbol{f}^{n+1}$, $(\varphi, \psi)_k = \int_{\Omega_k} \varphi\psi \, \mathrm{d}\boldsymbol{x}$, $k = 1, \ldots, K$.

The spectral element discretization proceeds by approaching the velocity space $L^2(\Omega)^2$ by its subspace of finite dimension X_N:

$$X_N = \{\boldsymbol{v} \in (L^2(\Omega))^2 :\ \boldsymbol{v}_k \in \mathbb{P}_N(\Omega_k)^2,\ k = 1, \ldots, K\}$$

and the pressure space $H^1(\Omega)/\mathbb{R}$ by M_N:

$$M_N = \{q \in C^0(\Omega)/\mathbb{R} :\ q_k \in \mathbb{P}_N(\Omega_k),\ k = 1, \ldots, K\}$$

(it is well known that the space M_N is subspace of $H^1(\Omega)/\mathbb{R}$). We consider the following spectral element discrete problem: *Find* $\boldsymbol{u}_N \in X_N$ and $P_N \in M_N$ *such that, for all* $\boldsymbol{v}_N \in X_N$ *and* $q_N \in M_N$,

$$\begin{aligned} &\alpha((\boldsymbol{u}_N, \boldsymbol{v}_N))_N + ((\omega_N \times \boldsymbol{u}_N, \boldsymbol{v}_N))_N + ((\nabla P_N, \boldsymbol{v}_N))_N = ((\underline{\boldsymbol{f}}, \boldsymbol{v}_N))_N, \\ &((\boldsymbol{u}_N, \nabla q_N))_N = 0, \end{aligned} \tag{20}$$

where the notation $((\cdot, \cdot))_N$ is defined in Eq. (17).

It is standard to write Eq. (20) more concisely in the abstract form: *Find* $\boldsymbol{u}_N \in X_N$ *and* $P_N \in M_N$ *such that,*

$$\begin{aligned} &a_N(\boldsymbol{u}_N, \boldsymbol{v}_N) + b_N(\boldsymbol{v}_N, P_N) = ((\underline{\boldsymbol{f}}, \boldsymbol{v}_N))_N \quad &\forall \boldsymbol{v}_N \in X_N, \\ &b_N(\boldsymbol{u}_N, q_N) = 0 \quad &\forall q_N \in M_N, \end{aligned} \tag{21}$$

where the bilinear forms a_N and b_N are defined as

$$a_N(\boldsymbol{u}_N, \boldsymbol{v}_N) = \alpha((\boldsymbol{u}_N, \boldsymbol{v}_N))_N + ((\omega \times \boldsymbol{u}_N, \boldsymbol{v}_N))_N \quad \forall \boldsymbol{u}_N, \boldsymbol{v}_N \in X_N \tag{22}$$

and

$$b_N(\boldsymbol{v}_N, q_N) = ((\nabla q_N, \boldsymbol{v}_N))_N \quad \forall \boldsymbol{v}_N \in X_N, \ \forall q_N \in M_N. \tag{23}$$

Theorem 3.1. *Problem* (21) *admits one unique solution.*

Proof. The proof of the theorem proceeds by verifying the four conditions of Lax-Milgram theorem: the continuity and the coercivity of the form a_N, the continuity and "Inf-Sup" condition of the form b_N.

The first three conditions are classical. We verify the Brezzi's "Inf-Sup" condition of the form $b_N(\boldsymbol{v}_N, q_N)$ as follows: given $q_N \in M_N$, then $q_{N,k} \overset{\text{def}}{=} q_N|_{\Omega_k}$ belongs to $\mathbb{P}_N(\Omega_k)$. Let $\boldsymbol{v}_{N,k} = \nabla q_{N,k}$, then $\boldsymbol{v}_{N,k} \in \mathbb{P}_N(\Omega_k)$. If $\boldsymbol{v}_N$ is defined such that $\boldsymbol{v}_N|_{\Omega_k} = \boldsymbol{v}_{N,k}$, we have $\boldsymbol{v}_N \in X_N$ and

$$\begin{aligned}
((\boldsymbol{v}_N, \nabla q_N))_N &= \sum_{k=0}^{K} (\boldsymbol{v}_{N,k}, \nabla q_{N,k})_{N,k} \\
&= \sum_{k=0}^{K} (\nabla q_{N,k}, \nabla q_{N,k})_{N,k} \\
&= \|\nabla q_N\|_N^2 \\
&= \|\boldsymbol{v}_N\|_N \|\nabla q_N\|_N
\end{aligned}$$

which means that the "Inf-Sup" condition:

$$\inf_{q_N \in M_N} \sup_{\boldsymbol{v}_N \in X_N} \frac{((\boldsymbol{v}_N, \nabla q_N))_N}{\|\boldsymbol{v}_N\|_N \|\nabla q_N\|_N} \geqslant \beta_N$$

holds with "Inf-Sup" constant $\beta_N = 1$.

The existence and the unicity of problem (21) is then a direct consequence of the saddle theory (see, e.g. Ref. [9]). □

Remark 3.2. In Eqs. (20) we do not impose any explicit interface conditions for the discrete velocity on Γ_k, $k = 1, \ldots, K$. Indeed the second equation of (20) implies that

$$\begin{aligned}
\boldsymbol{u}_{N,k} \cdot \boldsymbol{n}_k(\xi_{ij}^e) + \boldsymbol{u}_{N,l} \cdot \boldsymbol{n}_l(\xi_{ij}^e) = (\nabla \cdot \boldsymbol{u}_{N,k}(\xi_{ij}^e) + \nabla \cdot \boldsymbol{u}_{N,l}(\xi_{ij}^e)) w_{0,e}^1 \\
e, k, l = 1, \ldots, K \text{ such that } \xi_{ij}^e \in (\bar{\Omega}_k \cap \bar{\Omega}_l) \cap \Xi_N \backslash \{O, \boldsymbol{b}_e\}
\end{aligned}$$

where $w_{0,e}^1$ is the first weight corresponding to the interface Γ_e, $\boldsymbol{n}_k$ denotes the outward unit normal on $\partial\Omega_k$ related to subdomain Ω_k. Note that $w_{0,e}^1$ is proportional to $1/N^2$ which means that on the elemental interfaces, the spectral element discretization "naturally" generates a weak C^0 continuous condition of the velocity solution in the normal direction.

3.2. Hyperbolic problem in the vorticity ω

The vorticity ω is governed by the equations as follows:

$$\alpha\omega + (\boldsymbol{u}\cdot\nabla)\omega = g \quad \text{in } \Omega, \tag{24}$$

where $g = \alpha\omega^n + \nabla\times\boldsymbol{f}^{n+1}$.

We approximate problem (24) by *finding* $\omega_N \in E_N$, *such that*

$$\alpha((\omega_N, z_N))_N + \tfrac{1}{2}((\boldsymbol{u}_N\cdot\nabla\omega_N, z_N))_N + \tfrac{1}{2}((\nabla\cdot(I_N(\boldsymbol{u}_N\omega_N)), z_N))_N = ((g, z_N))_N \quad \forall z_N \in E_N, \tag{25}$$

where discrete space E_N is defined by

$$E_N = \{z_N \in C^0(\Omega);\ z_N|_{\Omega_k} \in \mathbb{P}_N(\Omega_k)\},$$

I_N is the Lagrange interpolation operator over the Gauss–Lobatto points. $\boldsymbol{u}_N$ is the discrete solution of the velocity computed precedently.

3.3. Global stability results

We have first a stability estimate for the solution of Problem (21).

Theorem 3.3. *Assuming* $\boldsymbol{u}_N$ *to be the solution of* (21), *the following stability estimate holds*

$$\alpha\|\boldsymbol{u}_N\|_N \leqslant \|\underline{\boldsymbol{f}}\|_N. \tag{26}$$

Proof. Taking $\boldsymbol{v}_N = \boldsymbol{u}_N$ in the first equation of (21) and using the second and the coercivity of the form a_N, we obtain

$$\alpha\|\boldsymbol{u}_N\|_N^2 = ((\boldsymbol{u}_N, \underline{\boldsymbol{f}}))_N$$

which gives Eq. (26) by appling the Schwartz inequality. □

For the discrete solution of problem (25), we need the following numerical technique.

Post-treatment: To deduce the stability estimate over the approached vorticity ω_N, we first introduce a post-treatment for the velocity $\boldsymbol{u}_N$ computed by Problem (20). This post-treatment procedure, on the one hand, permits to regularize the discrete velocity near the elemental interfaces, on the other hand it conducts to a better stability estimate for ω_N. It consists in averaging the values of $\boldsymbol{u}_{N,k}$ on both sides of each interface, and forcing $\boldsymbol{u}_{N,k}$ into zero (in our homogeneous case) on the real boundary $\partial\Omega$. Precisely we construct the post-treatment discrete solution $\underline{\boldsymbol{u}}_N$ as follows: supposing Ω_m and Ω_n are two adjacent subdomains on the interface Γ_k, then

$$\underline{\boldsymbol{u}}_{N,m}(\xi_{ij}^k) = \underline{\boldsymbol{u}}_{N,n}(\xi_{ij}^k) = \begin{cases} \dfrac{\boldsymbol{u}_{N,m}(\xi_{ij}^k) + \boldsymbol{u}_{N,n}(\xi_{ij}^k)}{2} & \forall \xi_{ij}^k \in \Xi_N \cap (\bar{\Gamma}_k \backslash \{O\}), \\ \frac{1}{K}\sum_{k=1}^K \boldsymbol{u}_{N,k}(\xi_{ij}^k) & \text{for } \xi_{ij}^k \in \Xi_N \cap \{O\}, \end{cases} \tag{27}$$

and

$$\underline{\boldsymbol{u}}_{N,k}(\xi_{ij}^k) = \begin{cases} \boldsymbol{u}_{N,k}(\xi_{ij}^k) & \forall \xi_{ij}^k \in \Xi_N \cap \Omega_k, \\ 0 & \forall \xi_{ij}^k \in \Xi_N \cap \partial\Omega. \end{cases} \tag{28}$$

An important question related to this post-treatment procedure is whether the post-treated solution is stable, in other words, if the equivalence between $\|\underline{\boldsymbol{u}}_N\|_N$ and $\|\boldsymbol{u}_N\|_N$ holds. In order to illustrate the equivalence we consider $K=2$ for simplicity, then

$$\begin{aligned}\sum_{k=1}^{2}\sum_{i,j=0}^{N}\underline{\boldsymbol{u}}_N^2(\xi_{ij}^k)w_{ij}^k &= \sum_{i,j=0}^{i=N-1,j=N}\boldsymbol{u}_N^2(\xi_{ij}^1)w_{ij}^1+\sum_{j=0}^{N}\left(\frac{\boldsymbol{u}_N(\xi_{Nj}^1)+\boldsymbol{u}_N(\xi_{0j}^2)}{2}\right)^2 w_{Nj}^1\\ &\quad+\sum_{j=0}^{N}\left(\frac{\boldsymbol{u}_N(\xi_{Nj}^1)+\boldsymbol{u}_N(\xi_{0j}^2)}{2}\right)^2 w_{0j}^2+\sum_{i=1,j=0}^{N}\boldsymbol{u}_N^2(\xi_{ij}^2)w_{ij}^2\\ &\leqslant \sum_{i,j=0}^{i=N-1,j=N}\boldsymbol{u}_N^2(\xi_{ij}^1)w_{ij}^1+\sum_{j=0}^{N}\frac{\boldsymbol{u}_N^2(\xi_{Nj}^1)}{2}(w_{Nj}^1+w_{0j}^2)\\ &\quad+\sum_{j=0}^{N}\frac{\boldsymbol{u}_N^2(\xi_{0j}^2)}{2}(w_{Nj}^1+w_{0j}^2)+\sum_{i=1,j=0}^{N}\boldsymbol{u}_N^2(\xi_{ij}^2)w_{ij}^2.\end{aligned}$$

In our case, we have

$$w_{Nj}^1=w_{0j}^2. \tag{29}$$

Therefore

$$\begin{aligned}\sum_{k=1}^{2}\sum_{i,j=0}^{N}\underline{\boldsymbol{u}}_N^2(\xi_{ij}^k)w_{ij}^k &\leqslant \sum_{i,j=0}^{i=N-1,j=N}\boldsymbol{u}_N^2(\xi_{ij}^1)w_{ij}^1+\sum_{j=0}^{N}\boldsymbol{u}_N^2(\xi_{Nj}^1)w_{Nj}^1\\ &\quad+\sum_{j=0}^{N}\boldsymbol{u}_N^2(\xi_{0j}^2)w_{0j}^2+\sum_{i=1,j=0}^{N}\boldsymbol{u}_N^2(\xi_{ij}^2)w_{ij}^2\\ &\leqslant \sum_{k=1}^{2}\sum_{i,j=0}^{N}\boldsymbol{u}_N^2(\xi_{ij}^k)w_{ij}^k,\end{aligned}$$

which gives

$$\|\underline{\boldsymbol{u}}_N\|_N\leqslant\|\boldsymbol{u}_N\|_N. \tag{30}$$

We state the following property.

Proposition 3.4. *The post-treated discrete solution $\underline{\boldsymbol{u}}_N$ has an equivalent estimate in discrete norm $\|\cdot\|_N$ to the solution $\boldsymbol{u}_N$ without the post-treatment.*

Theorem 3.5. *For ω_N, solution of Problem* (25) *with $\boldsymbol{u}_N$ replaced by $\underline{\boldsymbol{u}}_N$, the following stability estimate holds*

$$\|\omega_N\|_N\leqslant\|g\|_N. \tag{31}$$

We first prove the following equality:

Lemma 3.6. *For the post-treated discrete velocity* $\underline{\boldsymbol{u}}_N$ *and any* $\omega_N \in E_N$, *we have*

$$((\nabla \cdot (I_N(\underline{\boldsymbol{u}}_N \omega_N)), \omega_N))_N = -((\underline{\boldsymbol{u}}_N \cdot \nabla \omega_N, \omega_N))_N. \tag{32}$$

Proof. Using Definition (15) and the exact quadratic formula (17), we obtain

$$\begin{aligned}
&((\nabla \cdot (I_N(\underline{\boldsymbol{u}}_N \omega_N)), \omega_N))_N \\
&= \sum_{k=1}^{K} \sum_{j=0}^{N} \sum_{i=0}^{N} (\nabla \cdot (I_N(\underline{\boldsymbol{u}}_N \omega_N)))_{ij} \omega_{N,ij} w_{i,k}^1 w_{j,k}^2 \\
&= \sum_{k=1}^{K} \left[\sum_{j=0}^{N} \int_{I_{x_1}^k} \left(\frac{\partial I_N(\underline{\boldsymbol{u}}_N \omega_N)}{\partial x_1} \right)_j \omega_{N,j} w_{j,k}^2 \, \mathrm{d}x_1 + \sum_{i=0}^{N} \int_{I_{x_2}^k} \left(\frac{\partial I_N(\underline{\boldsymbol{u}}_N \omega_N)}{\partial x_2} \right)_i \omega_{N,i} w_{i,k}^1 \, \mathrm{d}x_2 \right] \\
&= -\sum_{k=1}^{K} \left[\sum_{j=0}^{N} \int_{I_{x_1}^k} I_N(\underline{\boldsymbol{u}}_N \omega_N)_j \frac{\partial \omega_{N,j}}{\partial x_1} w_{j,k}^2 \, \mathrm{d}x_1 + \sum_{i=0}^{N} \int_{I_{x_2}^k} I_N(\underline{\boldsymbol{u}}_N \omega_N)_i \frac{\partial \omega_{N,i}}{\partial x_2} w_{i,k}^1 \, \mathrm{d}x_2 \right] \\
&\quad + \sum_{k=1}^{K} \int_{\partial \Omega_k} (\underline{\boldsymbol{u}}_N \cdot \boldsymbol{n}_k) \omega_N^2 \, \mathrm{d}\sigma \\
&= -((\underline{\boldsymbol{u}}_N \cdot \nabla \omega_N, \omega_N))_N,
\end{aligned}$$

where $I_{x_i}^k$ denotes the intervals in the x_i direction of the subdomain Ω_k, $\varphi_{N,ij} = \varphi_N(\xi_{i,k}^1, \xi_{j,k}^2)$, $\varphi_{N,i} = \varphi_N(\xi_{i,k}^1, x_2)$ and $\varphi_{N,j} = \varphi_N(x_1, \xi_{j,k}^2)$. In the last passage, we have used the equality

$$\sum_{k=1}^{K} \int_{\partial \Omega_k} (\underline{\boldsymbol{u}}_N \cdot \boldsymbol{n}_k) \omega_N^2 \, \mathrm{d}\sigma = 0$$

due to the post-treatment (27)–(28) and the fact that $\omega_N \in H^1(\Omega)$ and $\underline{\boldsymbol{u}}_N \cdot \boldsymbol{n} = 0$. □

Proof of Theorem 3.5. Taking $z_N = \omega_N$ in Eq. (25) and using Eq. (32), we obtain

$$\sum_{k=1}^{K} \sum_{i,j=0}^{N} \omega_N^2(\xi_{ij}^k) w_{ij}^k \leqslant \sum_{k=1}^{K} \sum_{i,j=0}^{N} g(\xi_{ij}^k) \omega_N(\xi_{ij}^k) w_{ij}^k.$$

Estimate (31) is then obtained by appling the Schwarz inequality. □

Remark 3.7. In the case of nonhomogeneous boundary condition $\boldsymbol{u} \cdot \boldsymbol{n} = \varphi \neq 0$, we have an analogous estimate but more a boundary term appeared in each of the two sides. Hoping $\boldsymbol{u}_N$ to be sufficiently close to the continuous solution $\boldsymbol{u}$, we could also obtain the stability results.

4. Extension to more complex geometries

We consider only the $(\boldsymbol{u},P)$-problem for illustrating the extension techniques to more complex geometries. Extension for the ω-problem can be done in an analogous way.

It is well known that the efficiency of the spectral methods for resolution of the Navier–Stokes equations depends on the behavior of the "Inf-Sup" constant β_N. The constant β_N is associated to the pressure precision, and also to the convergence rate of algorithms (solvers) used. The optimal estimate of the "Inf-Sup" coefficient satisfies (see, e.g. Ref. [4]): $\beta_N \simeq 1/\sqrt{N}$.

In the resolution of the Euler equations, we are going to see that β_N is much more simple to estimate. Let us consider a general domain as it will only be assumed to be open and connected with a piecewise regular boundary. We assume, in addition, that a partition of the domain in curved rectangles is possible in such a way that: $\bar{\Omega} = \bigcup_{k=1}^{K} \bar{\Omega}_k$, $\Omega_k \cap \Omega_l = \emptyset$, $\forall k, l = 1,\dots,K$, $k \neq l$, and we also assume that the decomposition is geometrically conforming in the sense that the intersection of two adjacent elements is either a common vertex or a common entire edge.

We notice $\boldsymbol{F}_k$, a regular one-to-one mapping, from the reference square domain $\mathscr{C} = (-1,+1)^2$ to the subdomain Ω_k. The four edges $\Gamma_{k,j}$ of Ω_k are the images by $\boldsymbol{F}_k$ of the edges Γ_j of $\mathscr{C}$. We assume that the boundary $\partial\Omega$ is sufficiently piecewise regular so that $\boldsymbol{F}_k \in \mathscr{C}^\infty(\mathscr{C})$ and the Jacobian J_k (respectively $\tilde{J}_k$) of $\boldsymbol{F}_k$ (respectively $\boldsymbol{F}_k^{-1}$) is larger than some positive constant. In this geometrically conforming situation, we assume in addition that the restrictions of $\boldsymbol{F}_k$ and $\boldsymbol{F}_l$ on $\bar{\Omega}_k \cap \bar{\Omega}_l$ coincide.

The discrete space X_N corresponding to the continuous velocity will consist of functions that are piecewise continuous on each element Ω_k, $1 \leqslant k \leqslant K$, and such that their restriction to each Ω_k is an image, via $\boldsymbol{F}_k$, of some polynomial over $\mathscr{C}$; more precisely, X_N will be defined in the following way:

$$X_N = \{\boldsymbol{v} \in L^2(\Omega)^2;\ \boldsymbol{v} \circ \boldsymbol{F}_k \in \mathbb{P}_N(\mathscr{C})^2,\ k = 1,\dots,K\}.$$

The discrete space for the pressure, M_N, will be a subset of all continuous functions, defined by

$$M_N = \{q \in H^1(\Omega)/R;\ q \circ \boldsymbol{F}_k \in \mathbb{P}_N(\mathscr{C}),\ k = 1,\dots,K\}.$$

Remark 4.1. In the multidomain case where the geometry is rectilinear (i.e. $\boldsymbol{F}_k$ are only translations or affine mappings), as the one shown in Fig. 1, the definitions of X_N and M_N are equivalent to the ones defined precedently in this paper.

On discretization of Problem (7) we have

$$\sum_{k=1}^{K}\sum_{i=0}^{N}\sum_{j=0}^{N} \alpha(\boldsymbol{u}_N \circ \boldsymbol{F}_k)_{ij}(\boldsymbol{v}_N \circ \boldsymbol{F}_k)_{ij} J_k w_{ij}^k + \sum_{k=1}^{K}\sum_{i=0}^{N}\sum_{j=0}^{N} (\omega_N \times \boldsymbol{u}_N \circ \boldsymbol{F}_k)_{ij}(\boldsymbol{v}_N \circ \boldsymbol{F}_k)_{ij} J_k w_{ij}^k$$
$$+ \sum_{k=1}^{K}\sum_{i=0}^{N}\sum_{j=0}^{N} ((\nabla P_N) \circ \boldsymbol{F}_k)_{ij}(\boldsymbol{v}_N \circ \boldsymbol{F}_k)_{ij} J_k w_{ij}^k = \sum_{k=1}^{K}\sum_{i=0}^{N}\sum_{j=0}^{N} (\underline{f} \circ \boldsymbol{F}_k)_{ij}(\boldsymbol{v}_N \circ \boldsymbol{F}_k)_{ij} J_k w_{ij}^k$$
$$\forall \boldsymbol{v}_N \in X_N,$$

$$\sum_{k=1}^{K}\sum_{i=0}^{N}\sum_{j=0}^{N} (\boldsymbol{u}_N \circ \boldsymbol{F}_k)_{ij}((\nabla q_N) \circ \boldsymbol{F}_k)_{ij} J_k w_{ij}^k = 0 \quad \forall q_N \in M_N.$$

The well posedness of this problem relies on the same arguments as in the case of Fig. 1 domain. The first point is on the verification of the continuity and the ellipticity of the form a_N defined by

$$a_N(\boldsymbol{u}_N, \boldsymbol{v}_N) = \sum_{k=1}^{K}\sum_{i=0}^{N}\sum_{j=0}^{N} \alpha(\boldsymbol{u}_N \circ \boldsymbol{F}_k)_{ij}(\boldsymbol{v}_N \circ \boldsymbol{F}_k)_{ij} J_k w_{ij}^k$$

$$+ \sum_{k=1}^{K}\sum_{i=0}^{N}\sum_{j=0}^{N} (\omega_N \times \boldsymbol{u}_N \circ \boldsymbol{F}_k)_{ij}(\boldsymbol{v}_N \circ \boldsymbol{F}_k)_{ij} J_k w_{ij}^k \quad \forall \boldsymbol{u}_N, \boldsymbol{v}_N \in X_N,$$

as is proven in Ref. [2] or Ref. [1] for the Navier–Stokes equations, following the techniques used in Ref. [6], for the reasons:

(i) The mappings $\boldsymbol{F}_k$ are inversible and their Jacobians J_k are larger than a positive constant.

(ii) The Gauss–Lobatto quadratic formula satisfies Property (15).

The continuity of the form b_N defined by

$$b_N(\boldsymbol{v}_N, q_N) = \sum_{k=1}^{K}\sum_{i=0}^{N}\sum_{j=0}^{N} (\boldsymbol{v}_N \circ \boldsymbol{F}_k)_{ij}((\nabla q_N) \circ \boldsymbol{F}_k)_{ij} J_k w_{ij}^k \quad \forall \boldsymbol{v}_N \in X_N, \ q_N \in M_N$$

follows exactly from the same argument.

For the rectilinear domain (in the sense stated before), we have the following "Inf-sup" condition.

Lemma 4.2. *Assume that the geometry is rectilinear. Then the "Inf-Sup" constant* $\beta_N = 1$, *i.e.*

$$\inf_{q_N \in M_N} \sup_{\boldsymbol{v}_N \in X_N} \frac{b_N(\boldsymbol{v}_N, q_N)}{\|\boldsymbol{v}_N\|_N \|\nabla q_N\|_N} \geqslant 1.$$

In the more general case of a curved domain, we can show the compatibility between the spaces X_N and M_N.

Lemma 4.3. *There exists a positive constant* β *such that*

$$\inf_{q_N \in M_N} \sup_{\boldsymbol{v}_N \in X_N} \frac{b_N(\boldsymbol{v}_N, q_N)}{\|\boldsymbol{v}_N\|_{0,\Omega} |q_N|_{1,\Omega}} \geqslant \beta.$$

Proof. Denoting $\nabla_{(r,s)}$ the gradient operator in the reference domain $\mathscr{C}$, we can easily deduce the following equality:

$$b_N(\boldsymbol{v}_N, q_N) = \sum_{k=1}^{K}\sum_{i=0}^{N}\sum_{j=0}^{N} (\boldsymbol{v}_N \circ \boldsymbol{F}_k)_{ij}((\nabla q_N) \circ \boldsymbol{F}_k)_{ij} J_k w_{ij}^k$$

$$= \sum_{k=1}^{K}\sum_{i=0}^{N}\sum_{j=0}^{N} (\boldsymbol{v}_N \circ \boldsymbol{F}_k)_{ij}(\mathscr{J}_{F_k})^{-1}(\nabla_{(r,s)}(q_N \circ \boldsymbol{F}_k))_{ij} J_k w_{ij}^k$$

where $(\mathscr{J}_{F_k})^{-1}$ is the inverse of the Jacobian matrix $\mathscr{J}_{F_k}$ of the mapping $\boldsymbol{F}_k$. We know, from the proof of Theorem 3.1 that there exists $\boldsymbol{v}_N^\star = \nabla_{(r,s)}(q_N \circ \boldsymbol{F}_k)$ (nonpolynomial generally) such that

$$\sum_{k=1}^{K}\sum_{i=0}^{N}\sum_{j=0}^{N} \boldsymbol{v}_{N,ij}^\star (\nabla_{(r,s)}(q_N \circ \boldsymbol{F}_k))_{ij} w_{ij}^k > 0.$$

The question now is to know whether there exists a discrete function $\boldsymbol{v}_N \in X_N$, or reciprocally a polynomial $\boldsymbol{w}_N \equiv \boldsymbol{v}_N \circ \boldsymbol{F}_k \in \mathbb{P}_N(\mathscr{C})^2$ such that

$$\sum_{k=1}^{K}\sum_{i=0}^{N}\sum_{j=0}^{N} (\boldsymbol{v}_N \circ \boldsymbol{F}_k)_{ij} (\mathscr{J}_{F_k})^{-1} (\nabla_{(r,s)}(q_N \circ \boldsymbol{F}_k))_{ij} J_k w_{ij}^k$$
$$= \sum_{k=1}^{K}\sum_{i=0}^{N}\sum_{j=0}^{N} \boldsymbol{v}_{N,ij}^\star (\nabla_{(r,s)}(q_N \circ \boldsymbol{F}_k))_{ij} w_{ij}^k.$$

For that, we introduce the projection operator Π_N from $L^2(\mathscr{C})^2$ onto $\mathbb{P}_N(\mathscr{C})^2$ defined by

$$\sum_{k=1}^{K}\sum_{i=0}^{N}\sum_{j=0}^{N} (\Pi_N \boldsymbol{\phi} - \boldsymbol{\phi})_{ij} ((\mathscr{J}_{F_k})^{-1} J_k \boldsymbol{\psi}_N)_{ij} w_{ij}^k = 0 \quad \forall \boldsymbol{\phi} \in L^2(\mathscr{C})^2, \quad \forall \boldsymbol{\psi}_N \in \mathbb{P}_N(\mathscr{C})^2$$

which is well defined. We easily verify that the polynomial $\boldsymbol{w}_N \in \mathbb{P}_N(\mathscr{C})^2$:

$$\boldsymbol{w}_N = \Pi_N \left(\frac{\boldsymbol{v}_N^\star}{J_k} \mathscr{J}_{F_k} \right)$$

is the one that we are looking for. □

5. Numerical tests

We consider the evolutional Euler equations:

$$\frac{\partial \boldsymbol{u}}{\partial t} + \boldsymbol{u} \cdot \nabla \boldsymbol{u} + \nabla p = \boldsymbol{f}, \quad \nabla \cdot \boldsymbol{u} = 0,$$

in the domain showed in Fig.1. The solutions to approximate are the analytical functions:

$$u_1(x, y, t) = \cos\left(\frac{\pi x}{2}\right) \sin\left(\frac{\pi y}{2}\right) \cos(t),$$

$$u_2(x, y, t) = -\sin\left(\frac{\pi x}{2}\right) \cos\left(\frac{\pi y}{2}\right) \cos(t),$$

$$\omega(x, y, t) = -\pi \cos\left(\frac{\pi x}{2}\right) \cos\left(\frac{\pi y}{2}\right) \cos(t),$$

$$P(x, y, t) = x^2 + y^2.$$

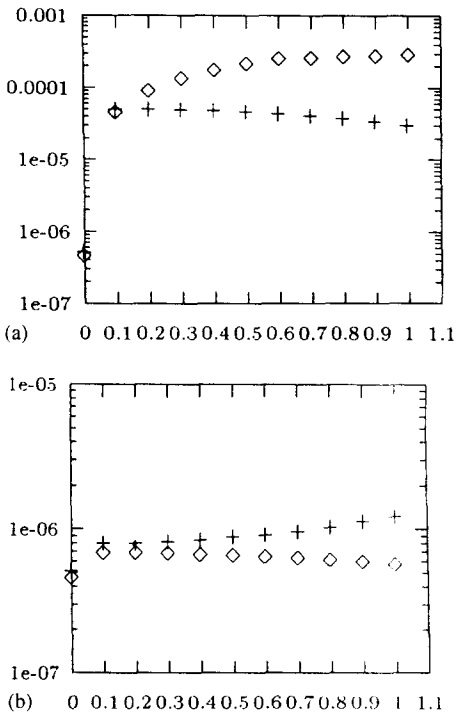

Fig. 2. (a) (left) A plot of $\|u-u_N^n\|_N(\diamond)$, $\|\omega-\omega_N^n\|_N(+)$ as a function of time $n\triangle t$, using 1-order time schema (4)–(5) with $\triangle t=0.001$. (b) A plot of $\|u-u_N^n\|_N(\diamond)$, $\|\omega-\omega_N^n\|_N(+)$ as a function of time $n\triangle t$, using 2-order time schema (33)–(34) with $\triangle t=0.001$.

In order to improve the time discretization accuracy, we use 1-order schema (4)–(5), and also a 2-order schema:

$$\frac{3u^{n+1}-4u^n+u^{n-1}}{2\triangle t}+(2\omega^n-\omega^{n-1})\times u^{n+1}+\nabla P^{n+1}=f^{n+1},\quad \nabla\cdot u^{n+1}=0, \tag{33}$$

$$\frac{3\omega^{n+1}-4\omega^n+\omega^{n-1}}{2\triangle t}(u^{n+1}\cdot\nabla)\omega^{n+1}=\nabla\times f^{n+1}. \tag{34}$$

The first numerical test is related to the determination of temporal discretization errors and proves the stability of the discrete solution. The polynomial degree is chosen large enough to allow elimination of all spatial errors, so errors in the solutions reflect only time differencing errors. In Fig. 2a we plot the discrete errors $\|u-u_N^n\|_N$ and $\|\omega-\omega_N^n\|_N$ as a function of time using 1-order temporal discretization. Fig. 2b plots $\|u-u_N^n\|_N$ and $\|\omega-\omega_N^n\|_N$ obtained by 2-order temporal schema. Note that in Fig. 2a, the errors behave as $O(\triangle t)$ while in Fig. 2b the errors behave as $O(\triangle t^2)$.

The second test concerns numerical investigation of the dependence of spatial discretization errors on the polynomial degree N. The 2-order time discretization schema (33)–(34) is used. Time step $\triangle t$ is now chosen small enough such that all time differencing errors are negligible, so errors in the solutions reflect only spatial discretization errors. Fig. 3 shows the spectral accuracy obtained.

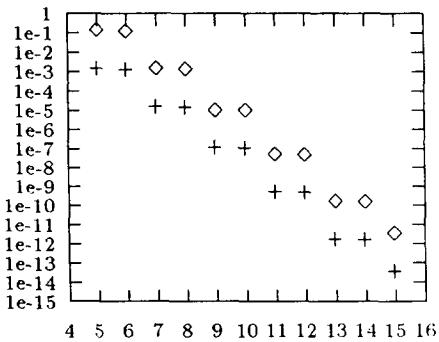

Fig. 3. A plot of $\|u-u_N^n\|_N(+)$, $\|\nabla(P-P_N^n)\|_N(\diamond)$ as a function of polynomial degree N. The results show the spectral accuracy obtained.

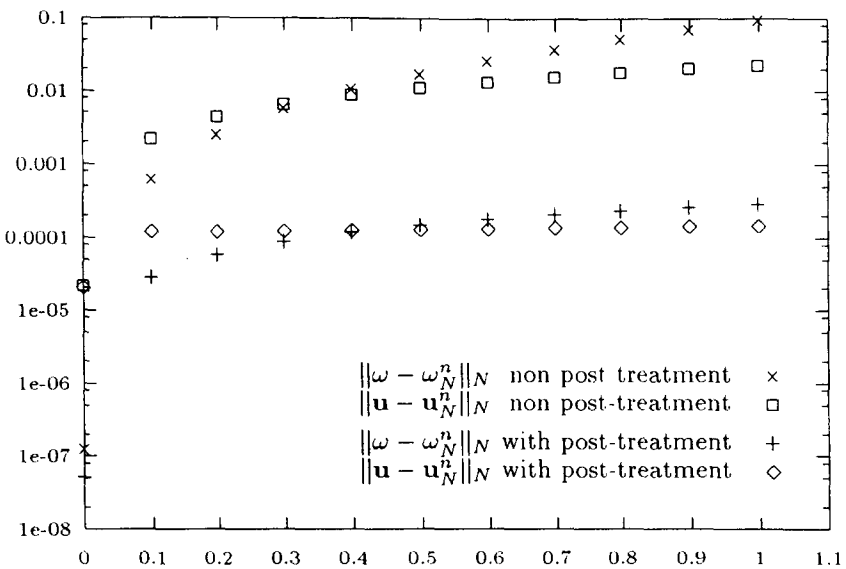

Fig. 4. A plot of $\|u-u_N^n\|_N$ and $\|\omega-\omega_N^n\|_N$ as a function of the time without (×,□) and with (+, ◇) post-treatment. Polynomial degree used is $N=11$, time step $\Delta t=0.001$.

In the above computation, we did not use the post-treatment (27)–(28). This suggests that the post-treatment is not really needed to solutions of high regularity (in this case effect of averaging the discrete velocities on interfaces is negligible).

However for solutions of lower regularity, the post-treatment (27)–(28) could be necessary, which is proven by the following numerical examples. Considering now the solutions:

$$u_1(x,y,t)=(1-y^2)^{3/2},$$
$$u_2(x,y,t)=0,$$
$$P(x,y,t)=x^{4/3}+y^{4/3}.$$

We effectuate an error comparison for the discrete solutions u_N^n and ω_N^n with or without post-treatment. Fig. 4 shows an error evolution of $\|u-u_N^n\|_N$ and $\|\omega-\omega_N^n\|_N$ as a function of time. Note

both the stability and accuracy are improved by the post-treatment. This confirms that the continuity of the velocity can stabilize the discrete vorticity ω_N, and hence improve the global approximation accuracy. In fact for all numerical examples we performed, better results are always obtained by computation procedure using the post-treatment technique.

6. Applications to flow simulation

We apply in this section the precedent method to some simulations of fluid flow. Although a large number of engineering and scientific applications involve incompressible inviscid fluid flow described by the Euler equations, we present delicate kind of applications of the approximation method proposed. The applications are based on a coupled model of the incompressible Navier–Stokes and Euler equations. As a particular implementation of domain decomposition ideas, the strategy of coupling viscous/inviscid models has received considerable attention in recent years. We cite among others [8, 14] for the compressible viscous/inviscid coupling in the context of finite element approximation, and [16, 17] for the incompressible viscous/inviscid equations in the context of spectral approximation. To understand what and how the computations will be done, we review the basic theoretical aspects of this coupling strategy.

Suppose that the computational domain Ω is broken into two subdomains Ω_- and Ω_+, with the interface $\Gamma = \partial\Omega_- \cap \partial\Omega_+$, $\Omega_- \cap \Omega_+ = \emptyset$. Let $\Gamma_k = \partial\Omega \cap \partial\Omega_k$, $k = -, +$. $\boldsymbol{n}_-, \boldsymbol{n}_+$ are the unit normals to Ω_-, Ω_+ respectively (so $\boldsymbol{n}_- = -\boldsymbol{n}_+$ on Γ). The model used is as follows:

$$
\begin{aligned}
&\frac{\partial \boldsymbol{u}_-}{\partial t} + (\boldsymbol{u}_- \cdot \nabla)\boldsymbol{u}_- - \nu\triangle \boldsymbol{u}_- + \nabla p_- = \boldsymbol{f}_- \quad \text{in } Q_-,\\
&\frac{\partial \boldsymbol{u}_+}{\partial t} + (\boldsymbol{u}_+ \cdot \nabla)\boldsymbol{u}_+ + \nabla p_+ = \boldsymbol{f}_+ \quad \text{in } Q_+,\\
&\boldsymbol{u}_-(0) = \boldsymbol{u}_-^0 \text{ in } \Omega_-, \qquad \boldsymbol{u}_+(0) = \boldsymbol{u}_+^0 \quad \text{in } \Omega_+,\\
&\boldsymbol{u}_-|_{\Sigma_-} = 0, \qquad \boldsymbol{u}_+ \cdot \boldsymbol{n}_+|_{\Sigma_+} = 0
\end{aligned}
\tag{35}
$$

with the incompressibility $\nabla \cdot \boldsymbol{u} = 0$, where $Q_k = \Omega_k \times (0,T)$, $\Sigma_k = \Gamma_k \times (0,T)$, $k = -, +$, $T > 0$, and $\boldsymbol{u}_-^0, \boldsymbol{u}_+^0$ are the initial conditions.

The nonlinear term is written in vorticity form, while the pressure p is replaced by the total pressure P. The matching conditions on the interfaces are

$$
\begin{aligned}
&\nu\frac{\partial \boldsymbol{u}}{\partial \boldsymbol{n}_-} - P_-\boldsymbol{n}_- = P_+\boldsymbol{n}_+ \quad \text{on } \Gamma,\\
&\boldsymbol{u}_- \cdot \boldsymbol{n}_- = -\boldsymbol{u}_+ \cdot \boldsymbol{n}_+ \qquad \text{on } \Gamma.
\end{aligned}
\tag{36}
$$

At each time iteration, the vorticity ω in the viscous domain (i.e., ω_-) is computed directly by setting $\omega_- = \nabla \times \boldsymbol{u}_-$; meanwhile the vorticity in the inviscid domain, ω_+, is computed by solving a transport equation with "inflow" boundary conditions given on the natural boundary Γ_+^{in} and also on the interface Γ^{in}, where $\Gamma^{\text{in}} = \{\boldsymbol{x} \in \Gamma;\ \boldsymbol{u}_+ \cdot \boldsymbol{n}_+(\boldsymbol{x}) < 0\}$.

Taking an example of 2-order time discretization, that is, we discretize Eqs. (35)–(36) as follows:

$$\frac{3\boldsymbol{u}_-^{n+1}-4\boldsymbol{u}_-^{n}+\boldsymbol{u}_-^{n-1}}{2\,\triangle t}-\nu\triangle\boldsymbol{u}_-^{n+1}+2(\nabla\times\boldsymbol{u}_-^{n})\times\boldsymbol{u}_-^{n}-(\nabla\times\boldsymbol{u}_-^{n-1})\times\boldsymbol{u}_-^{n-1}+\nabla P_-^{n+1}$$
$$=\boldsymbol{f}_-^{n+1}\quad\text{in }\Omega_-,$$
$$\frac{3\boldsymbol{u}_+^{n+1}-4\boldsymbol{u}_+^{n}+\boldsymbol{u}_+^{n-1}}{2\,\triangle t}+(2\omega_+^{n}-\omega_+^{n-1})\times\boldsymbol{u}_+^{n+1}+\nabla P_+^{n+1}=\boldsymbol{f}_+^{n+1}\quad\text{in }\Omega_+,$$
$$\nabla\cdot\boldsymbol{u}_-^{n+1}=0\quad\text{in }\Omega_-,\qquad\nabla\cdot\boldsymbol{u}_+^{n+1}=0\quad\text{in }\Omega_+,$$
$$\frac{3\omega_+^{n+1}-4\omega_+^{n}+\omega_+^{n-1}}{2\,\triangle t}+(\boldsymbol{u}_+^{n+1}\cdot\nabla)\omega_+^{n+1}=\nabla\times\boldsymbol{f}_+^{n+1}\quad\text{in }\Omega_+,$$
$$\nu\frac{\partial\boldsymbol{u}_-^{n+1}}{\partial\boldsymbol{n}_-}-P_-^{n+1}\boldsymbol{n}_-=P_+^{n+1}\boldsymbol{n}_+\quad\text{on }\Gamma,$$
$$\boldsymbol{u}_+^{n+1}\cdot\boldsymbol{n}_+=-\boldsymbol{u}_-^{n+1}\cdot\boldsymbol{n}_-\quad\text{on }\Gamma,$$
$$\omega_+^{n+1}=-\nabla\times\boldsymbol{u}_-^{n+1}\quad\text{on }\Gamma^{\text{in}},$$
$$\boldsymbol{u}_-^{n+1}|_{\Gamma_-}=0,\quad\boldsymbol{u}_+^{n+1}\cdot\boldsymbol{n}_+|_{\Gamma_+}=0,\quad\omega_+^{n+1}|_{\Gamma_+^{\text{in}}}=0,$$

in which $(\boldsymbol{u}_-^n,P_-^n)$ represents an approximation of $(\boldsymbol{u}_-(\boldsymbol{x},n\triangle t),P_-(\boldsymbol{x},n\triangle t))$ in the viscous subdomain, $(\boldsymbol{u}_+^n,P_+^n,\omega_+^n)$ represents an approximation of $(\boldsymbol{u}_+(\boldsymbol{x},n\triangle t),P_+(\boldsymbol{x},n\triangle t),\omega_+(\boldsymbol{x},n\triangle t))$ in the inviscid subdomain, and $\triangle t$ is the time step.

An essential computation in the above system lies on the resolution of the first three equations, which can be simplified into the following form (in dropping the time superscript $n+1$):

$$\begin{aligned}&\alpha\boldsymbol{u}_--\nu\triangle\boldsymbol{u}_-+\nabla P_-=\bar{\boldsymbol{f}}_-&&\text{in }\Omega_-,\\&\alpha\boldsymbol{u}_++\bar{\omega}_+\times\boldsymbol{u}_++\nabla P_+=\bar{\boldsymbol{f}}_+&&\text{in }\Omega_+,\\&\nabla\cdot\boldsymbol{u}_-=0\quad\text{in }\Omega_-,\quad\nabla\cdot\boldsymbol{u}_+=0&&\text{in }\Omega_+,\end{aligned}\tag{37}$$

where $\alpha=3/2\triangle t$, $\bar{\boldsymbol{f}}$ represents the corresponding source term, and $\bar{\omega}_+=2\omega_+^n-\omega_+^{n-1}$.

The well-posedness of Eqs. (37), completed by the interface conditions (36), has been investigated by the author in Ref. [17]. In the case of square computational domain, it is proven that the solution of the problem (37)–(36) can be exhibited as a limit of the solutions of two subproblems. Precisely, let $\boldsymbol{u}_-^0,\boldsymbol{u}_+^0$ to be two functions given in Γ, we define two sequences of function pair $(\boldsymbol{u}_-^m,P_-^m)_{m\geqslant1}$ and $(\boldsymbol{u}_+^m,P_+^m)_{m\geqslant1}$ by solving for each m (distinguished from the time superscript n) the following inviscid problem in Ω_+

$$\begin{aligned}&\alpha\boldsymbol{u}_+^m+\bar{\omega}_+\times\boldsymbol{u}_+^m+\nabla P_+^m=\bar{\boldsymbol{f}}_+,\qquad\nabla\cdot\boldsymbol{u}_+^m=0\quad\text{in }\Omega_+,\\&\boldsymbol{u}_+^m\cdot\boldsymbol{n}_+=0\quad\text{on }\Gamma_+,\quad\boldsymbol{u}_+^m\cdot\boldsymbol{n}_+=\varphi^m\quad\text{on }\Gamma,\end{aligned}\tag{38}$$

and then the following viscous problem in Ω_-:

$$\begin{aligned}&\alpha\boldsymbol{u}_-^m-\nu\triangle\boldsymbol{u}_-^m+\nabla P_-^m=\bar{\boldsymbol{f}}_-,\qquad\nabla\cdot\boldsymbol{u}_-^m=0\quad\text{in }\Omega_-,\\&\boldsymbol{u}_-^m=0\quad\text{on }\Gamma_-,\qquad\nu\frac{\partial\boldsymbol{u}_-^m}{\partial\boldsymbol{n}_-}-P_-^m\boldsymbol{n}_-=P_+^m\boldsymbol{n}_+\quad\text{on }\Gamma,\end{aligned}\tag{39}$$

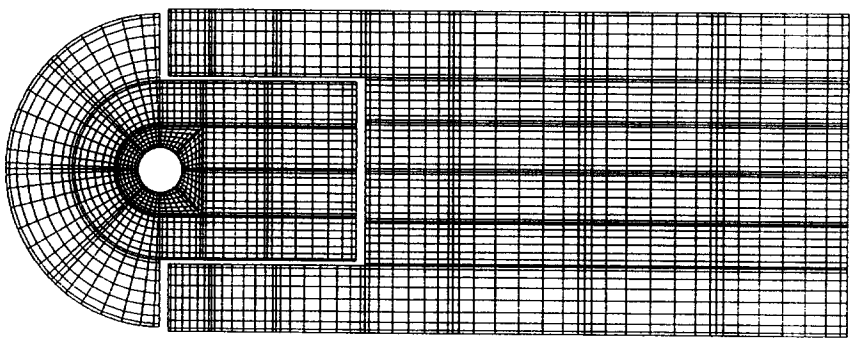

Fig. 5. Partition of domain and Gauss–Lobatto spectral element mesh used for the classical problem of flow, past a cylinder.

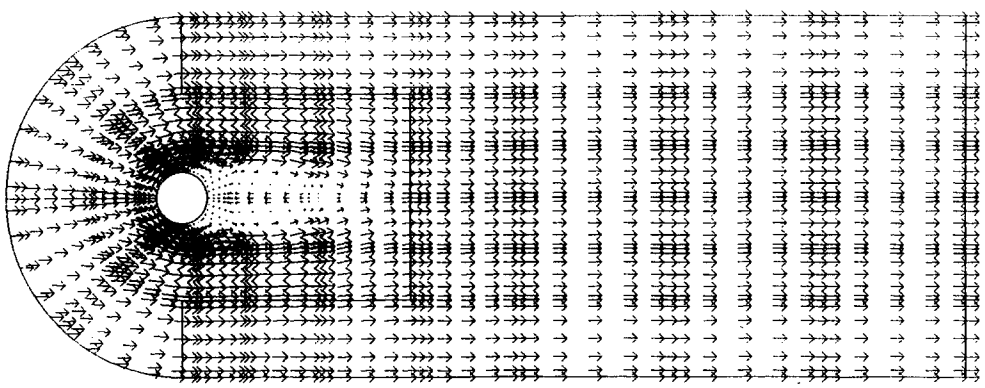

Fig. 6. A plot of the detailed velocity vector distribution for flow, past a cylinder at $Re = 100$ at $t = 5.871$.

where $\varphi^m = \theta \boldsymbol{u}_-^{m-1} \cdot \boldsymbol{n}_+|_\Gamma + (1-\theta)\boldsymbol{u}_+^{m-1} \cdot \boldsymbol{n}_+|_\Gamma$, satisfying the compatibility conditions $\int_\Gamma \varphi^m \, d\sigma = 0$, $\theta \in [0,1]$ is a relaxation parameter.

We generalize in this section the iteration-by-subdomain procedure to a more complex geometry, and apply it to flow simulations. Problem (39) is a standard Stokes problem with mixed Dirichlet–Neumann conditions, numerous spectral discretization methods can readily be applied. We choose the well known (optimal) $\mathbb{P}_N \times \mathbb{P}_{N-2}$ version [4]. Problem (38) is just the problem investigated in last sections of this paper, the method precedently presented is used in the spatial discretization.

We perform two series of simulations in which we try to capture the main features of flow when using our coupling model, as compared to the results obtained by using the pure viscous equations. In both tests the velocity is computed on the Gauss–Lobatto grid throughout the domain. The pressure in the Euler subdomain is also computed on the Gauss–Lobatto grid, while the pressure in the Navier–Stokes subdomain is computed on a staggered Gauss grid. For a sake of simplicity, we make the partition of domain according to physical and experimental considerations.

As our first example we consider the classical problem of flow, past a cylinder at a Reynolds number of $Re = U_\infty D/\nu = 100$, where U_∞ is the freestream velocity on the artificial boundary and D is the cylinder diameter. The initial flow velocity is set to the constant 1. Fig. 5 shows the

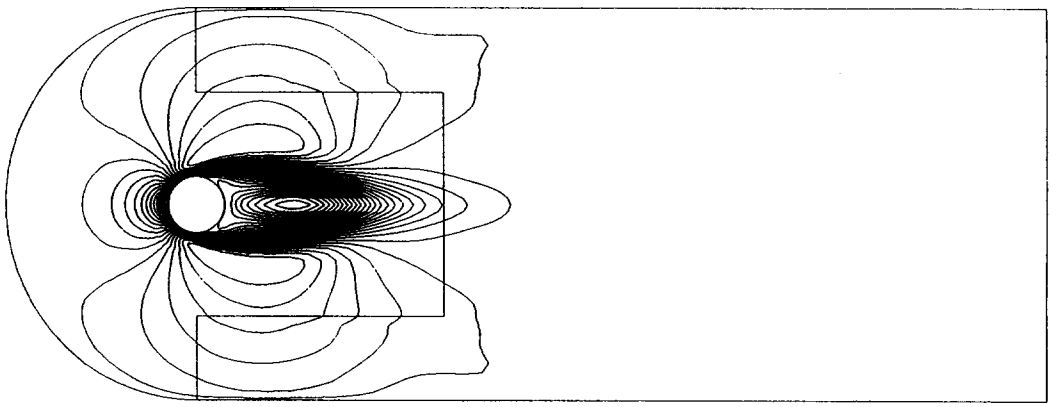

Fig. 7. Contourlines of the horizontal velocity of flow at $Re = 100$.

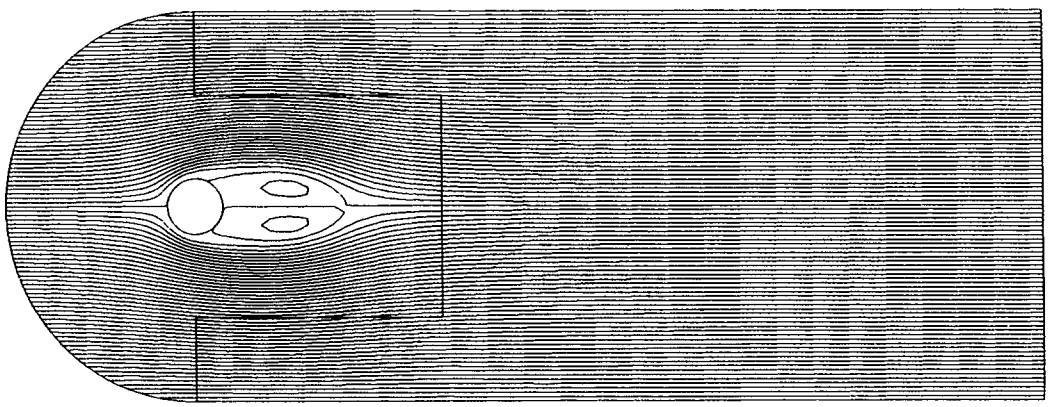

Fig. 8. A plot of the streamlines for flow, past a cylinder.

partition of the viscous and inviscid subdomains, and the Gauss–Lobatto–Legendre spectral element grid used. The end of the computational time is $t = 5.871$. Figs. 6 and 7, respectively, plot the instantaneous velocity vectors and contourlines of the horizontal velocity. The streamlines is given in Fig. 8. Note the continuity of the flow traversing the interface is obtained, which implicates that velocity interface relationship in Eq. (36) be satisfied. In Fig. 9 we present the contourlines of the pressure. We see that the pressure lines near the interface is smooth enough, which is indicative of the smallness of the viscous term in the interface relationship. Meanwhile we are very content with the fact that the numerical schema used remains stable, until effects of the outflow boundary become large.

In our second experiment we consider the problem of internal flow, past a stepped-channel with a step presented near the entry at a Reynolds number of $Re = U_{\max}(H - h)/v = 100$, where $U_{\max}$ is the maximum velocity on the entry boundary, H and h are respectively the height of the exit and the entry of the channel. The profile of the "inflow" boundary condition is taken as parabolic (Poiseuille flow). For simplifying our calculation we choose the "outflow" boundary condition of parabolic profile such that the incompressible compatibility condition be satisfied. The partition of the viscous

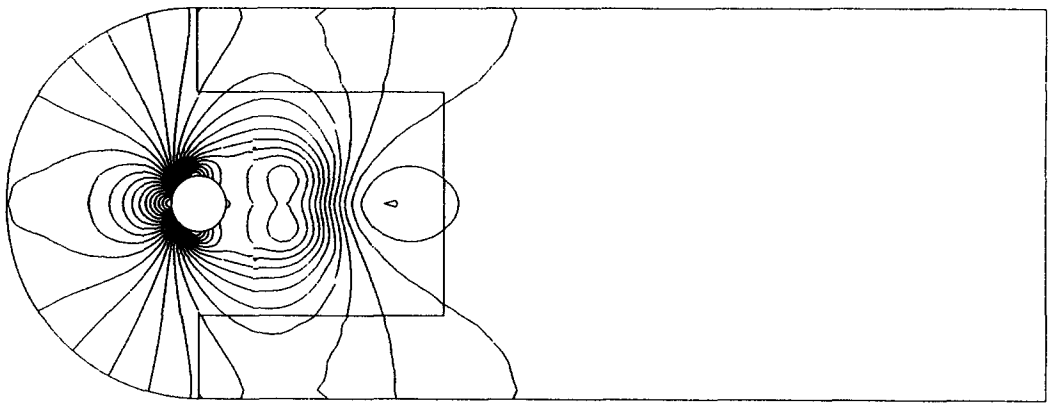

Fig. 9. Pressure contourlines for flow, past a cylinder.

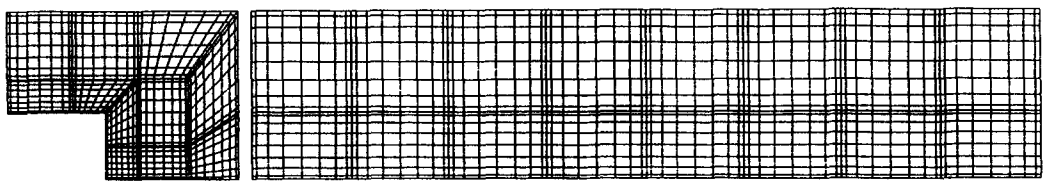

Fig. 10. Partition of domain and spectral element mesh used for the stepped-channel Poiseuille flow.

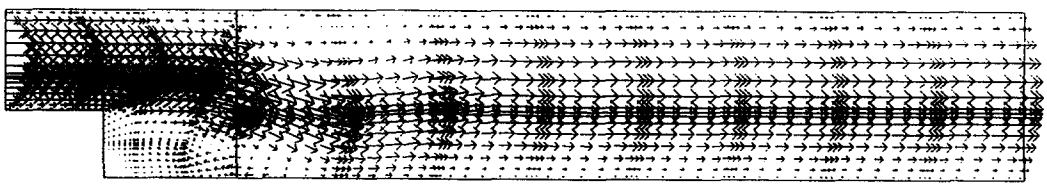

Fig. 11. Instantaneous velocity vectors distribution for the stepped-channel Poiseuille flow at $Re = 100$.

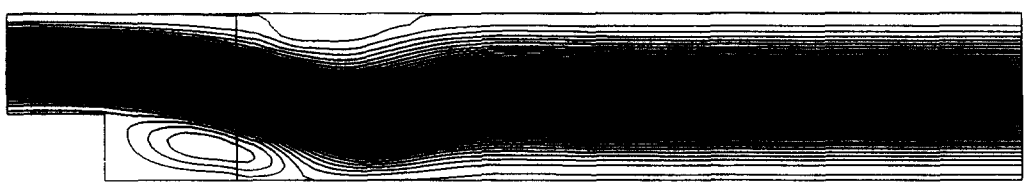

Fig. 12. A plot of the streamlines for the stepped-channel Poiseuille flow at $Re = 100$. The flow is essentially parallel with the exception of a small region corresponding to the wake of the step.

and inviscid subdomains and the Gauss–Lobatto spectral element mesh used in the calculation is shown in Fig. 10. Fine resolution is placed near the step in order to resolve the thin boundary layers and eddy structures expected in the vicinity of the step. In Figs. 11 and 12, we respectively plot the instantaneous velocity vectors and the steamlines at $t = 1.753$. Fig. 13 shows the contourlines of the horizontal velocity. The pressure contourlines at time 1.034 are ploted in Fig. 14. As in the first example, the continuity of the flow and the pressure traversing the interface is observable. Hence

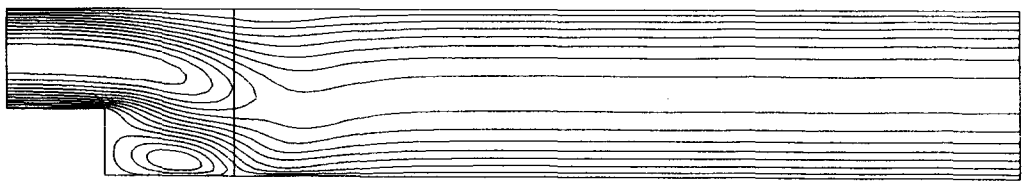

Fig. 13. Contourlines of the horizontal velocity. The continuity near the interface implicates the satisfaction of the interface conditions for the velocity solutions.

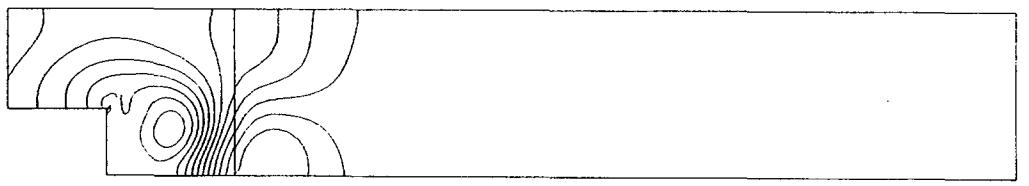

Fig. 14. Contourlines of the pressure. The continuity near the interface is indicative of the satisfaction of the interface conditions for the fluid flow.

we believe that the interface Γ has been taken sufficiently far from the effective viscous region for the time we computed, such that the resolution of our coupled model gives reasonable results, at least comparable to the results obtained by using the full Navier–Stokes equations within whole domain. In fact we have simultaneously resolved the pure Navier–Stokes equations throughout the entire (figures nonpresented in this paper), the results obtained do not have obvious difference.

7. Conclusion and discussion

We have established a stable numerical schema for the time-dependent incompressible Euler equations. In our schema, the temporal variable is discretized via a standard finite difference method while the spatial variable is discretized via a spectral element method. Approximation accuracy is proven by the numerical tests. Although it is known that in the approximation of coupled equations, interface interactions play an important role in destabilizing the numerical schema used, our flow simulations performed show that spectral element discretization for the Euler equations is stable even if coupled by the Navier–Stokes equations, provided correct matching conditions and appropriate post-treatment procedure be applied. The simulation results obtained with this coupling model show a reasonably good agreement with results obtained by using the pure Navier–Stokes equations (see also Refs. [7, 12]).

Concerning application of the viscous/inviscid coupled model, further developments will consist in:

(1) *Optimizing the locations of the artificial interface boundaries.* In view of reducing overall computational cost, it is desirable to take interface boundaries as close as possible to a region where the viscous effect is "small". A realizable procedure would be to use an adaptive mesh following an initial idea proposed by Brezzi et al. [3]. According to the point of view of Brezzi et al., locations of the artificial interface boundaries could be determined via computing the distribution of the values of $\nu \triangle \boldsymbol{u}$. Precisely, neglecting the diffusion effects in the Navier–Stokes equations is justified only in

the region where the divergence of the stress tensor is negligible, that is if, for a constant Reynolds number, $(1/Re)\triangle \boldsymbol{u}$ is negligible. This means that even for moderate Reynolds number, it is still possible to reduce the Navier–Stokes equations to the Euler equations in the region where $(1/Re)\triangle \boldsymbol{u}$ is smaller than an optimistic estimate of the discretization error. A first step toward this direction can be found in Ref. [15].

(2) Applying our viscous/inviscid coupled model to the research of the eddy-promoter stability theory related to viscous/inviscid analysis (see, e.g., [11, 10] and references therein). In particular, it could be applied to determine if the viscous mean flows induced by eddy-promoter are inviscidly unstable, or if they still require the Tollmien–Schlichting viscous mechanism to achieve positive growth rates.

References

[1] G. Anagnostou, Nonconforming sliding spectral element methods for the unsteady incompressible Navier–Stokes equations, Ph.D.Thesis, Massachusetts Institute of Technology, Cambridge, MA, 1991.

[2] G. Anagnostou, Y. Maday, C. Mavriplis, A.T. Patera, On the mortor element method: generalizations and implementation, In: Third International Symposium On Domain Decomposition Methods For Partial Differential Equations (Houston, 1989), SIAM, Philadelphia, 1990, pp. 157–173.

[3] F. Brezzi, C. Canuto, A. Russo, A self-adaptive formulation for the Euler/Navier–Stokes coupling, Comput. Meth. Appl. Mech. Engng. 73 (1989) 317.

[4] C. Bernardi, Y. Maday, Approximations spectrales de problèmes aux limites elliptiques, Collection Mathématiques et applications, vol. 10, Springer, New York, 1992.

[5] C. Canuto, M.Y. Hussaini, A. Quarteroni, T.A. Zang, Spectral Methods in Fluid Dynamics, Springer, New York, 1987.

[6] P.G. Ciarlet, P.A. Raviart, The combined effect of curved boundaries and numerical integration in isoparametric finite element methods, in: Aziz (Ed.), The Mathematical Foundations of the Finite Element Method with Applications to Partial Differential Equations, Academic Press, New York, 1972, p. 409.

[7] N. Debit, Coupling of spectral methods and finite element methods: resolution of the Navier–Stokes equations, Ph.D. Thesis, Université Pierre et Marie Curie, Paris, 1992.

[8] F. Gastaldi, A. Quarteroni, G. Sacchi Landriani, Effective methods for the treatment of interfaces separating equations of different character, in: G.M. Carlomagno, C.A. Brebbia (Eds.), Computers and Experiments in Fluid Flow, Springer, Berlin, 1989, pp. 65–74.

[9] V. Girault, P.A. Raviart, Finite Element Approximation of the Navier–Stokes Equations, Springer, New York, 1987.

[10] G.E. Karniadakis, C.H. Amon, Stability calculations of wall bounded flows in complex geometries, in: Proceedings of 6th IMACS Internat. Symp. on Comput. Mech. for Partial Differential Equations, 1987, p. 525.

[11] G.E. Karniadakis, B.B. Mikic, A.T. Patera, Minimum-dissipation transport enhancement by flow destabilization: Reynolds' analogy revisited, J. Fluid. Mech. 192 (1988) 365–394.

[12] Y. Maday, A.T. Patera, Spectral element methods for the Navier–Stokes equations, State-of-the-art Surveys in Computational Mechanics, A.K. Noor (Ed.), ASME, New York, 1988, pp. 71–143.

[13] Y. Maday, C.J. Xu, Une méthode spectrale pour les équations d'Euler bidimensionnelle, in: Internat. Conf. on Spectral And High Order Methods, Montpellier, France, 1992.

[14] L.D. Marini, A. Quarteroni, A relaxation procedure for domain decomposition methods using finite elements, Numer. Math. 55 (1989) 575–598.

[15] C.J. Xu, Couplage des équations de Navier–Stokes et d'Euler: Résolution par une méthode des éléments spectraux Ph.D. Thesis, Université Pierre et Marie Curie, Paris, 1993.

[16] C.J. Xu, An iterative method for the Navier–Stokes/Euler coupled equations, J. Comput. Math., 1998, to appear.

[17] C.J. Xu, Y. Maday, Coupling of the Euler and Navier–Stokes equations; Resolution by a spectral method, in: Proceedings of internat. Conf. on Engineering and Scientific Computing, Defence industrial press, Beijing, 1994, pp. 243–247.